Nano Res. 2011, 4(1): 103–114
DOI 10.1007/s12274-010-0058-9
Research Article

ISSN 1998-0124
CN 11-5974/O4

Self-Assembly and Photocatalysis of Mesoporous TiO_2 Nanocrystal Clusters

Qiao Zhang, Ji-Bong Joo, Zhenda Lu, Michael Dahl, Diana Q. L. Oliveira, Miaomiao Ye, and Yadong Yin (✉)

Department of Chemistry, University of California, Riverside, California 92521, USA

Received: 31 July 2010 / Revised: 24 August 2010 / Accepted: 12 October 2010

ABSTRACT

Mesoporous nanocrystal clusters of anatase TiO_2 with large surface area and enhanced photocatalytic activity have been successfully synthesized. The synthesis involves the self-assembly of hydrophobic TiO_2 nanocrystals into submicron clusters, coating of these clusters with a silica layer, thermal treatment to remove organic ligands and improve the crystallinity of the clusters, and finally removing silica to expose the mesoporous catalysts. With the help of the silica coating, the clusters not only maintain their small grain size but also keep their mesoporous structure after calcination at high temperatures (with BET surface area as high as 277 m^2/g). The etching of SiO_2 also results in the clusters having high dispersity in water. We have been able to identify the optimal calcination temperature to produce TiO_2 nanocrystal clusters that possess both high crystallinity and large surface area, and therefore show excellent catalytic efficiency in the decomposition of organic molecules under illumination by UV light. Convenient doping with nitrogen converts these nanocrystal clusters into active photocatalysts in both visible light and natural sunlight. The strategy of forming well-defined mesoporous clusters using nanocrystals promises a versatile and useful method for designing photocatalysts with enhanced activity and stability.

KEYWORDS

Mesoporous, titanium dioxide, photocatalysis, self-assembly, nitrogen doping, nanocrystals

1. Introduction

Clean and sustainable solar energy has been extensively explored in order to overcome the increasingly serious energy and environmental challenges. Among numerous approaches, chemical utilization of solar energy through photocatalysis has been recognized as one of the most promising methods [1–5]. Since the discovery of water splitting on the surface of titanium dioxide (TiO_2) electrodes under UV light irradiation [6], TiO_2 has been the most widely used photocatalyst in practical applications, including water splitting, water purification, and carbon dioxide conversion, due to its favorable features such as low cost, good chemical and mechanical stability, high photocatalytic activity, and non-toxic nature [7–16]. Three polymorphs of crystalline TiO_2—rutile, anatase, and brookite—occur in nature, of which anatase and rutile are usually employed as photocatalysts, while the photocatalytic activity of brookite has been little investigated. In photocatalysis, anatase TiO_2 is more active than the rutile crystalline form which has been

Address correspondence to yadong.yin@ucr.edu

attributed to its lower charge recombination rate and higher surface adsorption affinity for organic compounds [17–19]. Anatase TiO_2 is thermodynamically metastable and transforms to the rutile phase at high temperature (~600 ˚C).

The harvesting of solar energy by a TiO_2 photocatalyst can be roughly described in three sequential steps: (1) generation of electron–hole (e^-–h^+) pairs upon absorption of photons; (2) charge separation and migration to the catalyst surface; and (3) surface redox reactions. Much effort has been devoted to developing highly active TiO_2-based photocatalysts, with the aim of trying to improve the performance in some of these three steps [20–22]. For example, the main drawback of a pristine anatase TiO_2 photocatalyst is its large band gap energy (~3.2 eV) which allows it to absorb only UV light. As a result, many researchers have focused on developing visible-light-active TiO_2 photocatalysts that can make use of both UV (290–400 nm) and visible (400–700 nm) radiation to enhance process efficiencies. Dye-sensitization has been employed to extend the absorption from the UV range to the visible range. Organic dyes are usually transition metal complexes with low lying excited states, including polypyridine complexes, phthalocyanines, and metalloporphyrins [23–26]. However, the promise of such dye-sensitized TiO_2 materials and devices for practical applications is still under debate because of the instability of organic dyes on light irradiation [27]. Metal-ion doping is another popular method to make visible-light-active TiO_2-based photocatalysts. In many cases, however, these suffer from a serious deterioration in their photocatalytic performance because the metal ions themselves can act as the recombination centers of e^- and h^+ [28–30]. It has been demonstrated recently that doping with non-metals, including N, C, P, and S, can be useful in preparing visible-light-active TiO_2-based photocatalysts, even though an understanding of the origin of the enhanced activity is still controversial [27, 31–34]. On the other hand, the improved absorption of photons may not necessarily guarantee better photocatalytic performance because the efficiency of a photocatalyst is also determined by the charge separation and transportation step during the photoexcitation process. Due to the fast recombination of e^-–h^+ pairs, most excited charges recombine and are quenched before they can reach the surface. From this point of view, small crystal size and high crystallinity are desirable in order to enhance charge separation efficiency. Small crystal size can reduce the migration distance of charges, leading to a lower recombination rate. Another favorable consequence of small crystal size is the large surface area, which may improve the performance in the last step because it can provide more reactive sites. High crystallinity can also reduce the number of defects, which normally act as recombination centers. Since the rise of nanotechnology in the 1990s, great efforts have been made to synthesize semiconductor nanoparticles in order to enhance their specific surface area and, consequently, their catalytic activity. Many methods have been developed to synthesize TiO_2 nanoparticles [35], but further thermal treatment of the TiO_2 nanocrystals is usually needed to improve their crystallinity and photocatalytic activity. Owing to the large surface area and high surface energy of nanocrystals, thermal treatment at high temperatures usually causes ripening or fusion of small nanoparticles and finally leads to larger particles with a reduced surface area, which leads to a deterioration in the overall photocatalytic performance. It is thus of great importance to prepare highly efficient photocatalysts with high crystallinity and large surface area.

Mesoporous structures of TiO_2 represent another type of photocatalyst which promises high efficiency due to their large surface area. However, there are great challenges in preparing mesoporous anatase TiO_2 which possesses both large surface area and high crystallinity. Although it has been possible to produce TiO_2 mesoporous materials with large surface area by carrying out the sol–gel process with surfactant templates, a heat treatment step is usually required to convert the products into a crystalline anatase phase, which causes collapse of mesopores and a marked decrease in the surface area. Typically reported values [36, 37] of Brunauer–Emmett–Teller (BET) surface area for mesoporous TiO_2 materials are around 100 m^2/g, which is much smaller than that of their amorphous counterparts. Additionally, due to the uncontrollable pore collapse during the heat treatment process, it is also difficult to control the pore size distribution, which is important in some catalysis applications.

Recently, we and other groups reported a general strategy for the fabrication of novel porous nanostructured materials based on the self-assembly of nanocrystals [38–40]. We have demonstrated that the as-prepared mesoporous nanocrystal clusters can be used for selective enrichment of peptides and proteins from complex biological samples [40–42]. From the perspective of photocatalysis, there are also several attractive features of these materials, including clean surfaces, high crystallinity, small grain size, and large surface area even after high temperature treatment, good water dispersity, and a pore size distribution which is controllable by simply tuning the initial nanocrystal size and shape. Herein, we report their use as highly efficient and stable photocatalysts by taking advantage of this unique combination of features. Hydrophobic anatase TiO_2 nanocrystals were synthesized through a nonhydrolytic solution-based reaction. An emulsion-based bottom-up assembly approach was then used to self-assemble the colloidal nanocrystals into densely packed clusters by evaporating the low-boiling-point oil phase. After coating with a shell of silica, the as-obtained clusters were calcined at high temperature to improve their crystallinity and remove the organic ligands. Subsequent etching of the SiO_2 shell by an alkaline solution can remove the outer silica layer and give the TiO_2 cluster a hydrophilic surface, which allows better water accessibility to the pores. As a result of the calcination process, the mesoporous TiO_2 cluster retains its porous structure after the etching step. By optimizing the synthesis conditions, principally the calcination temperature, TiO_2 clusters with good photocatalytic activity have been obtained. It is believed that the enhanced photocatalytic performance comes from the unique cluster structure and the post-treatment steps of silica coating and etching, which results in small grains of TiO_2 clusters (~5 nm), large surface area, and hydrophilic surfaces. An N-doping process was also carried out in order to make the clusters catalytically active under irradiation by visible light. The catalytic activities of the mesoporous photocatalysts for the degradation of organic pollutants under UV, visible light, and direct sunlight were investigated using rhodamine B (RhB) as a model compound.

2. Experimental

2.1 Chemicals

Trioctylphosphine oxide (TOPO), sodium dodecyl sulfate (SDS), ammonium hydroxide solution (NH_4OH, ~28% NH_3 in water), tetraethylorthosilicate (TEOS, 98%), and rhodamine B (RhB, 99%) were purchased from Aldrich Chemical Co. Tetrabutylorthotitanate (TBOT) and titanium tetrachloride ($TiCl_4$) were obtained from Fluka. Ethanol (denatured), toluene, sodium hydroxide, cyclohexane, and acetone were obtained from Fisher Scientific.

2.2 Synthesis of TiO_2 nanocrystals

TiO_2 nanocrystals were prepared by a nonhydrolytic solution-based reaction [43]. Typically, TOPO (5 g) was heated at 150 ℃ for 5 min in vacuum to remove any low boiling point materials. After increasing the temperature to 200 ℃ under N_2 atmosphere, TBOT (1.4 mL) was injected into the hot liquid. The resulting mixture was then heated to 320 ℃, followed by a rapid addition of 0.55 mL of $TiCl_4$. The solution was kept at 320 ℃ for 20 min to ensure complete reaction. After cooling to 80 ℃, 10 mL of acetone was added to yield a white precipitate, which was isolated by centrifugation and subsequently washed with a toluene/acetone mixture to remove excess TOPO. The resulting powder was re-dispersed in 10 mL of cyclohexane.

2.3 Self-assembly of nanocrystals into clusters

The clusters were formed by assembling the nanocrystals in emulsion oil droplets and subsequent evaporation of the low-boiling-point solvent (the oil phase). In a typical process, 1 mL of a cyclohexane solution of nanocrystals was mixed with an aqueous solution of sodium dodecyl sulfate (SDS) (56 mg in 10 mL H_2O) under sonication for 5 min. The mixture was then heated at 70–72 ℃ in a water bath for 4 h. A clear nanoparticle solution was obtained by evaporating the cyclohexane. The reaction solution was cooled to room temperature and the final product was washed three times with water and re-dispersed in 3 mL of distilled water.

2.4 Surface modification of the clusters

TiO_2 nanocrystal clusters were coated with a layer of SiO_2 by using a modified Stöber process [44]. Typically, the above aqueous solution of TiO_2 clusters (3 mL) was first mixed with ethanol (20 mL) and ammonium hydroxide (1 mL, 28% aqueous solution). Then TEOS (0.1 mL) was injected into the solution and reacted for 20 min under vigorous stirring. The core/shell colloids were collected by centrifugation and washed three times with ethanol. After drying under vacuum overnight, the precipitate was heated to the desired temperature at a rate of 1 ℃ /min and heated for 1 h in air to remove the organic species. In the cases where N-doping was needed, the TiO_2@SiO_2 core–shell particles were heated under a NH_3/Ar flow in a Lindberg/Blue M tube furnace to the desired temperature at a rate of 1 ℃/min and heated for another hour to ensure the successful nitrogen doping and removal of organic species. The calcined particles were then dispersed in aqueous NaOH solution (5 mL, 0.5 mol/L) for 3–4 h with stirring, in order to dissolve the silica shell. The particles were collected by centrifugation and washed three times with distilled water.

2.5 Characterization

A Tecnai T12 transmission electron microscope (TEM) was used to characterize the morphology of the colloids in each step. Samples dispersed in ethanol at an appropriate concentration were cast onto a carbon-coated copper grid, followed by evaporation under vacuum at room temperature. The crystal structures of the samples were evaluated by X–ray diffraction (XRD), carried out on a Bruker D8 Advance diffractometer with Cu $K\alpha$ radiation (λ = 1.5418 Å). The surface area and porosity of the products were estimated by measuring the nitrogen adsorption–desorption isotherms on a Micromeritics ASAP 2020M Accelerated Surface Area and Porosimetry System. UV/Vis diffuse reflectance spectra were measured on a Shimadzu UV 3101PC double-beam, double-monochromator spectrophotometer. $BaSO_4$ powder was used as a reference (100% reflectance). A probe-type Ocean Optics HR2000CG-UV-NIR spectrometer was used to measure the UV–Vis absorption spectra of solutions in order to monitor the concentration of RhB at different time intervals. A three-electrode system (VersaSTAT 4, Princeton Applied Research) was utilized to characterize the electrochemical properties of the photocatalysts by using Ag/AgCl as the reference electrode, Pt wire as the counter electrode, and TiO_2 catalysts deposited on a 1-cm^2 ITO glass as the working electrode. An aqueous solution of RhB and Na_2SO_4 was used as the electrolyte.

2.6 Photocatalytic activity measurements

Photocatalytic degradation of RhB was carried out in a 100-mL beaker, containing 50 mL of reaction slurry agitated by magnetic stirring (650 r/min). The as-obtained TiO_2 clusters were first irradiated by UV light for 1 h to completely remove any residual organic ligands, followed by drying in an oven at 60 ℃ for 2 h. The aqueous slurry, prepared with different catalysts and 1.0×10^{-5} mol/L RhB was stirred in the dark for 30 min to ensure that the RhB was adsorbed to saturation on the catalysts. For the UV irradiation experiment, a 15 W UV lamp (254 nm, XX-15G, USA), 6 cm above the reaction slurry, was used as UV radiation source. The average light intensity striking the surface of the reaction solution was ~1.55 $mW \cdot cm^{-2}$. The concentration of titania was 200 mg/L for all the runs. For the visible light irradiation experiment, a 150 W tungsten lamp was used as the light source, and a cutoff filter was used to block the UV light (< 400 nm). The reaction flask was placed in a cooling water system to keep the reaction system at room temperature. To explore the photocatalytic performance in sunlight, the reaction flask was exposed directly to natural sunshine.

3. Results and discussion

The synthesis of TiO_2 nanocrystals involves a solution phase nonhydrolytic reaction between the two precursors TBOT and $TiCl_4$, with TOPO as both the solvent and surfactant [43]. The particle size as well as the morphology of the as-prepared TiO_2 nanocrystals can be simply tuned by varying the concentration of reactants and surfactants. Figure 1(a) shows a TEM image of a typical sample of TiO_2 nanocrystals

with an average diameter of 5 nm. The hydrophobic nanocrystals were dissolved in cyclohexane and then dispersed in water to form an oil-in-water emulsion with SDS acting as the surfactant. Upon evaporation of the low-boiling-point solvent (cyclohexane in this case), the nanocrystals confined in the oil droplets self-assembled into microspheres, with the size being controllable by adjusting the nanocrystal concentration or the extent of ultrasonication during emulsification (Fig. 1(b)). Generally, the lower the concentration of TiO_2 nanocrystals and the longer the sonication time, the smaller the size of the as-obtained TiO_2 clusters. The inset in Fig. 1(b) shows an enlarged TEM image of a single cluster, from which one can clearly appreciate the porous nature of the structure. The clusters were then successfully coated with a silica layer by a modified sol–gel process, as confirmed by the TEM image shown in Fig. 1(c). The thickness of the coated silica layer can be easily controlled by adjusting the amount of TEOS. Calcination of the resulting TiO_2/SiO_2 core–shell structure in air removes the organic ligands and improves the crystallinity as well as the mechanical stability. Finally, the silica layer was etched away to re-expose TiO_2 clusters by using a dilute solution of NaOH. The clusters retained their spherical shape and porous nature after the calcination and etching treatments (Fig. 1(d)), suggesting they have the good mechanical stability required for photocatalytic applications.

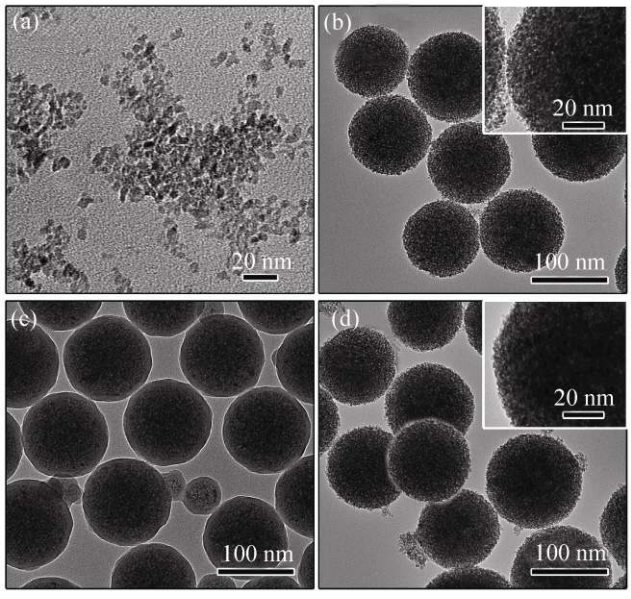

Figure 1 TEM images showing the preparation process of TiO_2 nanocrystal clusters: (a) TiO_2 nanocrystals; (b) self-assembled TiO_2 nanocrystal clusters; (c) SiO_2-coated TiO_2 clusters; (d) TiO_2 clusters after calcination of (c) at 400 ˚C for 1 h and subsequent removal of the SiO_2 shell by etching in NaOH. The insets in (b) and (d) are higher magnification images of the nanocrystal clusters

The crystallographic phases of the as-prepared catalysts were studied by recording their XRD patterns. As shown in Fig. 2, all the reflection peaks of the TiO_2 clusters can be indexed as a pure anatase structure with cell parameters $a = b = 3.78$ Å, $c = 9.51$ Å, in good agreement with the literature value (JCPDS card No. 21-1272). The peaks are all broad, indicating that the clusters are composed of small nanocrystals, which is consistent with the TEM observations. For all the samples, calcination at higher temperatures did not change the crystallographic phase of the as-prepared clusters, while the grain size of the clusters increased slightly during the calcination process. The Scherrer formula was used to estimate the average grain sizes of the TiO_2 clusters

$$D = \frac{0.89\lambda}{\beta \cos\theta} \quad (1)$$

where D is the diameter of the grains, λ the X-ray wavelength in nanometers ($\lambda = 0.15418$ nm in this case), β the width of the XRD peak at the half-peak height in radians, and θ the angle between the incident and diffracted beams in degrees. Figure 2(a) shows the XRD patterns of TiO_2 clusters after silica coating, calcination at different temperatures, and then silica etching. The grain size of the TiO_2 nanocrystals gradually increased from the initial value of 4.8 nm to about 5.5 nm for the sample calcined at 500 ˚C for 1 h. In contrast, as shown in Fig. 2(b), the TiO_2 nanocrystal clusters without silica protection underwent an increase in grain size to 6.9 nm at 400 ˚C and 8.4 nm at 500 ˚C, clearly suggesting that the silica shell has a protecting effect. The limited size increase of the nanocrystals in silica-protected clusters during calcination favors the retention of the anatase phase even after high-temperature treatment, as the grain size is still well below the critical value of 14 nm at which the anatase phase transforms to the rutile phase [45, 46].

As the surface-to-volume ratio of catalysts has a critical effect on their overall catalytic efficiency, the

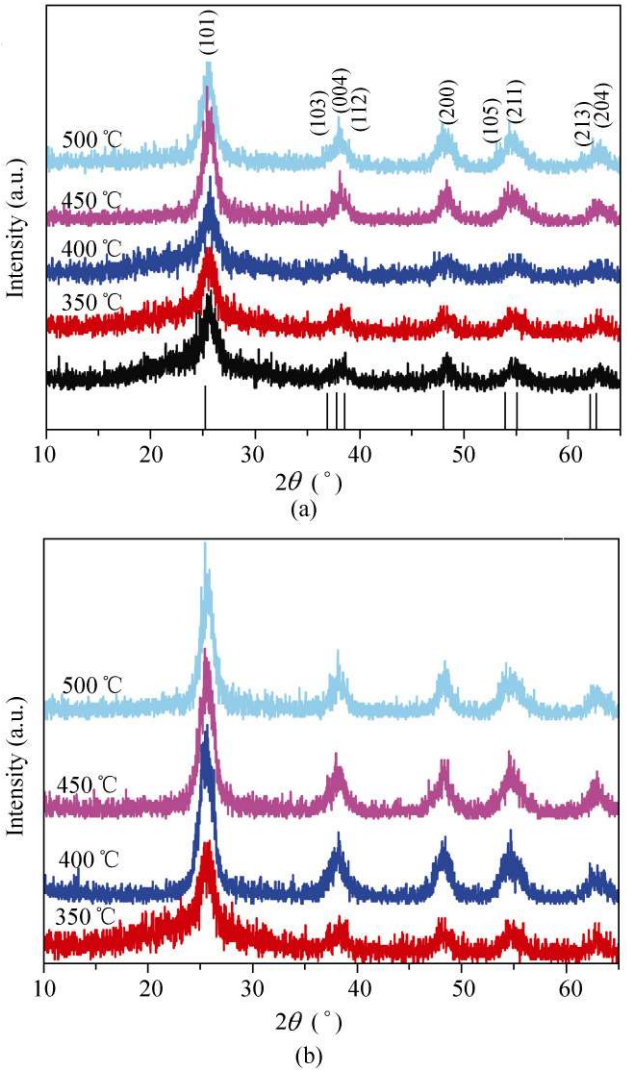

Figure 2 (a) XRD patterns of self-assembled TiO_2 clusters after calcination at different temperatures: 350 ˚C (TC350), 400 ˚C (TC400), 450 ˚C (TC450), and 500 ˚C (TC500). The black curve is for a sample prepared without calcination. All samples were prepared by sequential steps of self-assembly in emulsion droplets, silica coating, calcination, and silica etching. (b) XRD patterns of self-assembled TiO_2 clusters without silica protection after calcination at different temperatures

surface area, and porosity of the TiO_2 clusters after calcination at different temperatures were investigated by measuring their nitrogen adsorption–desorption isotherms. Figure 3(a) shows the nitrogen adsorption–desorption isotherms and the corresponding pore size distribution of the TiO_2 clusters calcined at 400 ˚C (TC400). The average pore diameter, as determined by using the Barrett–Joyner–Halenda (BJH) method on the desorption branch of the isotherm (inset of Fig. 3), increases slightly from 2.1 nm to 2.3 nm, and 2.4 nm after calcination at 350, 400, and 500 ˚C. The BET surface areas also decreased slightly with increasing calcination temperature, from 277 m^2/g for the sample treated at 350 ˚C to 268 m^2/g at 400 ˚C, and 253 m^2/g at 500 ˚C. Both changes can be ascribed to the gradual increase in grain size during calcination. We note that silica coating can help to maintain the mesoporous structure and therefore the large surface area of the clusters. As shown in Fig. 3(b), although the clusters without the silica coating still retained their mesoporous structure after calcination at 400 ˚C for 1 h, their surface area decreased markedly to 137 m^2/g, which is consistent with the significant grain growth of the unprotected samples during calcination.

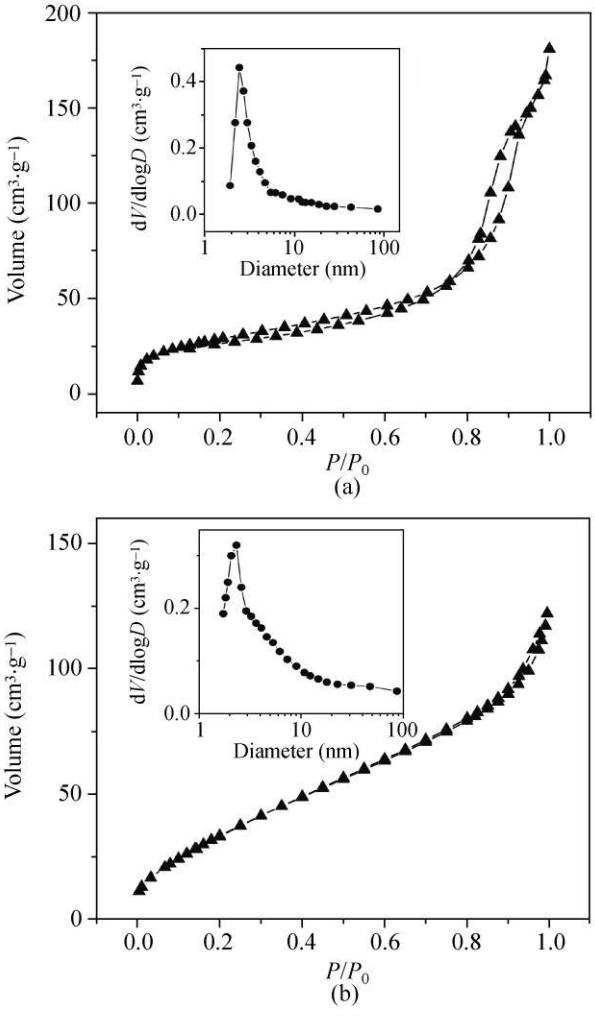

Figure 3 Nitrogen adsorption–desorption isotherms of TiO_2 clusters after calcination at 400 ˚C: (a) a layer of silica was coated on the clusters before calcination, and removed afterwards; (b) clusters were calcined without the silica treatment. The insets show the BJH pore size distribution of the corresponding samples

Electrochemical characterization was carried out to investigate the potential for use of the TiO_2 nanocrystal clusters in photocatalysis. Electrochemical impedance spectroscopy (EIS) was performed to characterize electrochemical interfacial reactions, in which the photocatalytic decomposition of RhB was used as the model reaction. A three-electrode system was utilized to measure the EIS spectrum by using Ag/AgCl as the reference electrode, Pt wire as the counter electrode, and TiO_2 catalyst deposited on ITO glass as the working electrode. An aqueous solution of RhB and Na_2SO_4 was used as the electrolyte. Figure 4(a) shows the EIS Nyquist plots under UV irradiation for AEROXIDE® P25 TiO_2 and the TiO_2 clusters calcined at different temperatures. It is well accepted that a smaller arc radius of an EIS Nyquist plot implies a higher efficiency of charge separation. Of the five samples, P25 TiO_2, and TC400 show the smallest arc radii, suggesting they have the highest charge separation efficiency. The relative charge separation efficiency increases in the order TC350 < TC500 < TC450 < TC400 ≈ P25.

Chronoamperometry (CA) experiments were used to characterize the photogenerated current density under a potential of 0.8 V and a periodic illumination of UV light. The photogenerated current density is usually regarded as equivalent to photocatalytic activity. As shown in Fig. 4(b), each of the five samples shows a photogenerated current, indicating their active response to UV irradiation. The shape of the CA curves was maintained after many cycles of light illumination, implying good photocatalytic stability. The current densities are consistent with the EIS measurements, with TC400 showing the highest value (~1.5 μA/cm^2).

The catalytic activity of the photocatalysts was evaluated by measuring degradation rates of RhB under irradiation by different light sources. Figure 5(a) shows typical absorption spectra of an aqueous solution of RhB exposed to UV light for various time periods using TC400 as the catalyst. The strong absorption peak at 553 nm gradually diminished in intensity as the UV irradiation was prolonged, and completely disappeared after 30 min, suggesting the complete photodegradation of the organic dye. The changes in RhB concentration (C) over the course of

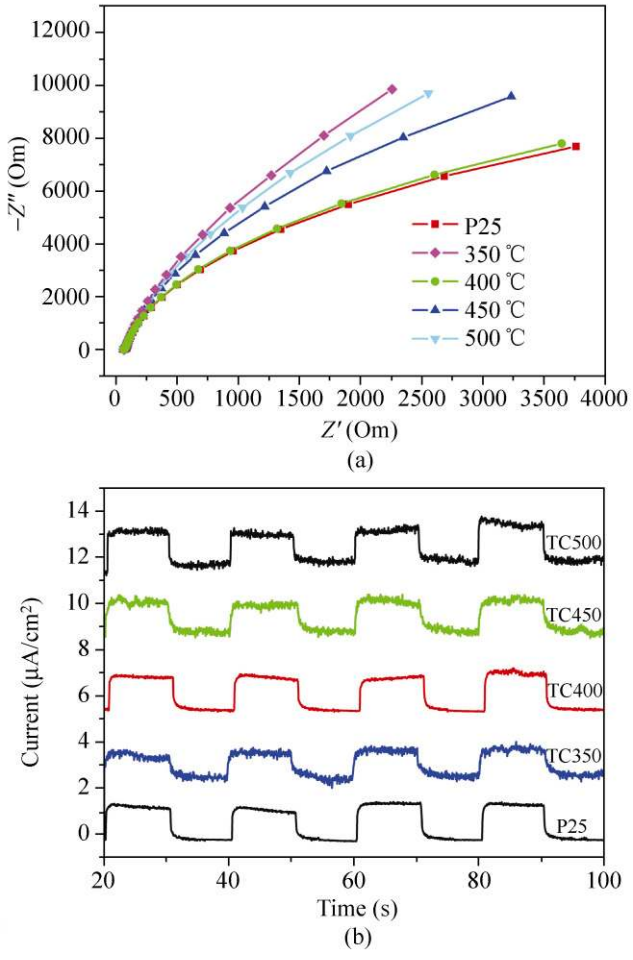

Figure 4 (a) Nyquist plots for P25 and TiO_2 clusters calcined at different temperatures in an aqueous solution of RhB under UV light illumination. Symbols and lines indicate the experimental data and fitted curves, respectively. (b) Chronoamperometry study of P25 and TiO_2 clusters calcined at different temperatures

photocatalytic degradation reactions using different photocatalysts subjected to the silica coating/removal process are summarized in Fig. 5(b). The photocatalysts were first illuminated by UV light for 1 h to rule out the influence of any organic residues in the cluster. To compare the photocatalytic activities, the total amount of TiO_2 was kept the same. Before illuminating the mixture it was stirred in the dark for 30 min to ensure that the RhB was adsorbed to saturation on the catalysts. The adsorption of RhB decreased for TiO_2 clusters treated at higher temperatures, while P25 showed the lowest adsorption due to its smallest surface area (~50 m^2/g). This is consistent with the BET measurements, which showed the surface area decreasing with increasing calcination temperatures.

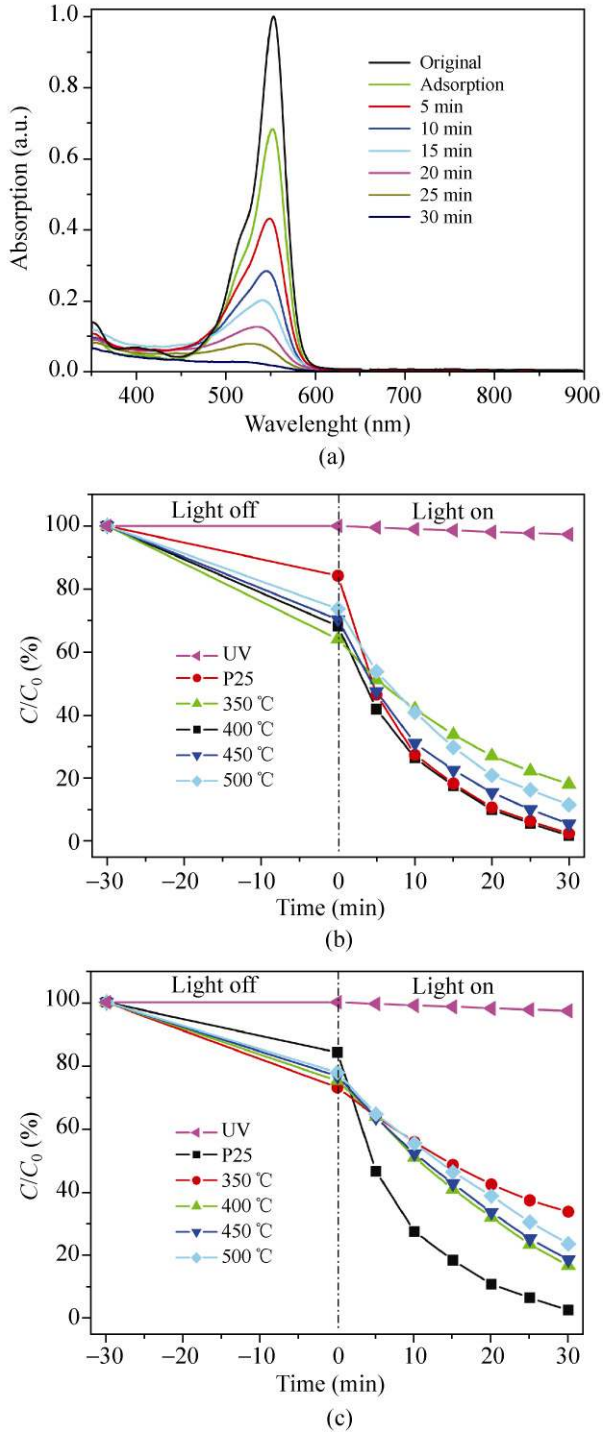

Figure 5 (a) UV absorption spectra showing the gradual decomposition of RhB under 254-nm UV irradiation in the presence of TiO_2 porous catalysts (calcined at 400 ℃). Photocatalytic conversion of RhB under UV irradiation by using TiO_2 clusters calcined at different temperatures and P25 as the photocatalysts: (b) the TiO_2 clusters were coated with a layer of silica before calcination, which was removed afterwards; (c) the clusters were calcined without silica treatment

However, the photocatalytic activity did not follow this simple trend. Although it showed the highest adsorption, the photocatalytic activity of TC350 was the lowest, probably due to its relatively low crystallinity. TC400 gave the highest photocatalytic activity, equivalent to that of P25, while TC450 showed similar activity to TC400 under UV irradiation in spite of its lower adsorption ability. Calcination at higher temperature resulted in reduced efficiency, as evidenced by the performance of TC500. Generally, higher photocatalytic activity is favored by larger surface area and the higher crystallinity of a catalyst. As pointed out above, higher calcination temperature leads to an improvement in the crystallinity by removing defects in the nanocrystals, but it also leads to a smaller surface area. It is apparent that calcination at an intermediate temperature of 400 ℃ is optimal for preparing mesoporous TiO_2 clusters with large surface area and relatively high crystallinity. The overall photocatalytic performance of the TiO_2 clusters is consistent with the results of electrochemical measurements.

We also studied the effect of the silica coating/removal process on the catalytic performance of the TiO_2 nanocrystal clusters. Compared to the samples treated with silica, clusters without silica protection during calcination showed much lower adsorption of RhB, as shown in Fig. 5(c). During the initial adsorption process, ~30% of RhB was adsorbed by the silica-treated clusters, while only 20% of RhB could be adsorbed by the untreated clusters. We have pointed out previously that the silica coating and etching processes enhances the surface charge and water dispersity of such clusters [40], which is confirmed by these experiments. Without the silica coating/removing treatment, the calcined TiO_2 clusters are in the form of large aggregates and cannot be well dispersed in water even after 10 min of sonication, while the silica-treated clusters can be well dispersed in water. Furthermore, as discussed above, the silica coating can help to maintain the mesoporous structure and therefore the large surface area of the clusters, which also favors a higher photocatalytic activity.

The porous structure of the TiO_2 nanocrystal clusters allows convenient nitrogen doping under NH_3/Ar gas flow. After reaction at the desired temperature, the

white powder became yellowish, suggesting successful nitrogen doping, which was further confirmed by measuring the diffuse reflectance UV–Vis spectra. Figure 6 shows the UV–Vis spectra of three samples: P25, and TiO_2 clusters before and after N-doping (NTC400). Compared with P25 and the undoped TiO_2 clusters that absorb only UV light, a noticeable shift of the absorption edge to the visible region was observed for the N-doped sample. To quantitatively study the influence of the N-doping process, the band gap energy change was calculated. As TiO_2 is a crystalline indirect transition semiconductor, the band gap energy of undoped and N-doped TiO_2 clusters can be estimated from the following equation

$$\alpha h\nu = A(h\nu - Eg)^{\gamma} \quad (2)$$

where α is the absorption coefficient, $h\nu$ is the energy of the incident photon, A is a constant, Eg is the optical energy gap of the material, and γ is a characteristic of the optical transition process which depends on whether the transition is symmetry allowed or not [47, 48]. The calculations show that the N-doping process does only red-shift the absorption edge, as evidenced by the second gap at 2.85 eV, but also reduces the main band edge from 3.2 eV to about 3.05 eV.

The successful N-doping process was also confirmed by the active response of the material under visible light irradiation. The degradation of RhB under visible light illumination was used as a model system to study the catalytic performance of the catalysts, as shown in Fig. 7(a). Upon illumination by visible light ($\lambda > 400$ nm) for 5 h, there was almost no change in the concentration of RhB if no catalyst was present, ruling out any possible sensitization process of RhB under visible light irradiation. The calcination temperature showed a significant influence on the photocatalytic activity, which is in good agreement with the results of irradiation by UV light. Due to the presence of rutile titania that can absorb visible light, the conversion of RhB using P25 as the catalyst was about 40% with an irradiation period of 5 h. Consistent with the data for the undoped samples, NTC400 showed the highest efficiency of all the calcined samples under the same conditions due to its optimal crystallinity and surface area: ~50% of the RhB was removed in the same period.

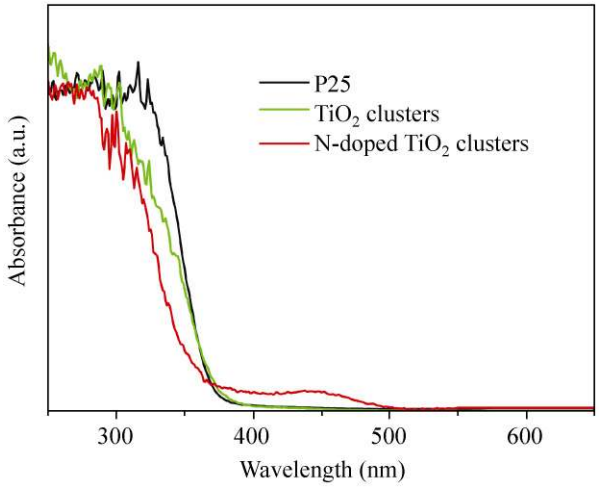

Figure 6 UV–Vis diffuse reflectance absorption spectra of P25, TiO_2 clusters (TC400), and N-doped TiO_2 clusters (calcined at 400 ˚C, denoted NTC400)

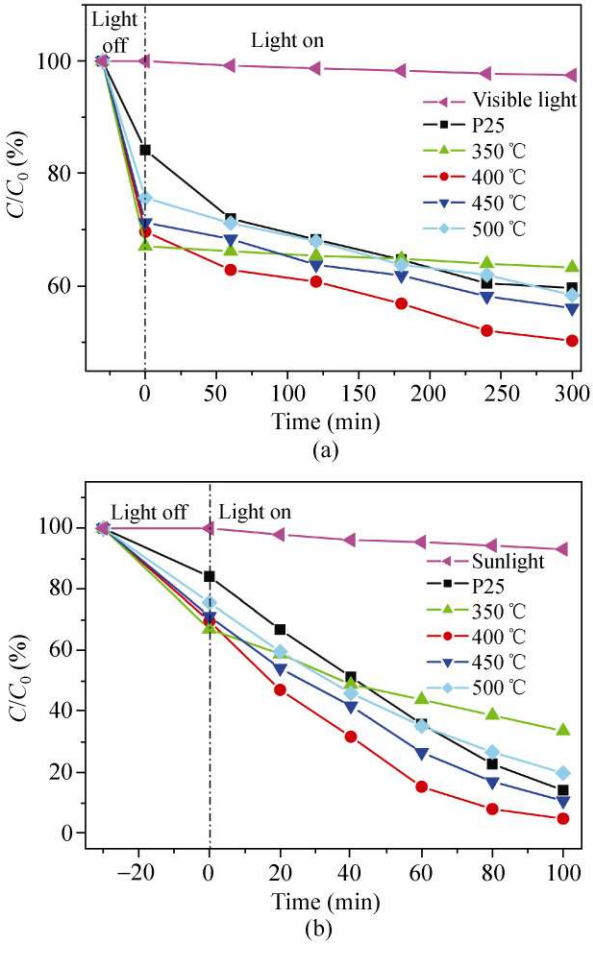

Figure 7 Photocatalytic conversion of RhB under (a) visible light irradiation ($\lambda > 400$ nm) and (b) illumination by direct sunlight using no catalyst, P25, and N-doped TiO_2 clusters calcined at different temperatures as the photocatalysts

To explore the photocatalytic activity of the as-prepared products for real applications in the photodegradation of organic pollutants, the photodegradation of RhB was also investigated under natural sunlight. As shown in Fig. 7(b), no sensitization of RhB was observed on illumination by sunlight. Commercial P25 showed higher activity compared to that under irradiation by pure visible light due to the contribution of the UV component in sunlight. With the aid of the cluster-structured photocatalysts, the sunlight can efficiently decompose RhB. As shown in Fig. 7(b), when using NTC400 as the photocatalyst, decomposition of RhB was complete within 100 min—much shorter than the time required under illumination by visible light. Consistent with the previous results for both UV and visible irradiation, NTC350 showed the lowest activity, while NTC450 and NTC500 showed lower activities than NTC400, which had the maximum activity.

As recyclability is very important for a catalyst, we also demonstrated that the cluster-structured photocatalysts can be recovered and reused to catalyze degradation under direct sunlight. Photocatalysis was performed in an aqueous solution over many cycles by repeatedly adding RhB and irradiating with natural sunlight. To ensure that RhB was completely removed and had no influence on the next cycle, further direct sunlight irradiation for 1 h was conducted after each cycle was complete. Centrifugation was used to recover the photocatalyst from the aqueous solution. As shown in Fig. 8, the catalyst did not exhibit any significant loss of photocatalytic activity after seven cycles. The slight differences in the extent of decomposition of RhB in different cycles might be caused by variations in the intensity of the sunlight.

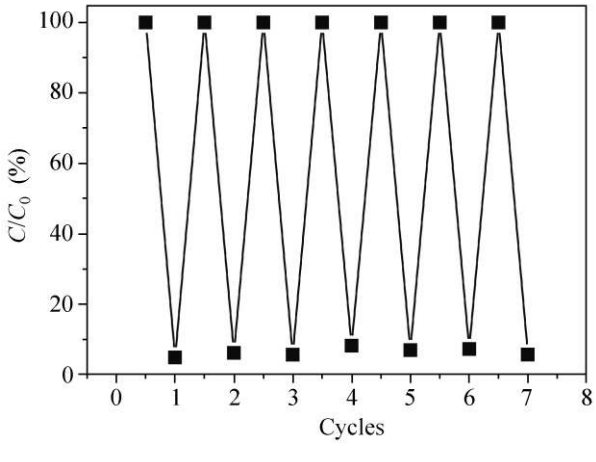

Figure 8 Seven cycles of photocatalytic degradation of RhB in the presence of NTC400 clusters under direct irradiation by sunlight

4. Conclusion

We have demonstrated the preparation of mesoporous anatase TiO_2 nanocrystal clusters with large surface area and enhanced photocatalytic activity. The synthesis involves the self-assembly of hydrophobic TiO_2 nanocrystals into submicron clusters in emulsion droplets, coating of these clusters with a silica layer, thermal treatment at high temperatures to remove the organic ligands and improve the crystallinity of clusters, and finally etching of the silica to reveal the mesoporous catalyst. The initial silica coating helps the clusters maintain their small grain size and high surface area after calcination at high temperatures, while the eventual removal of the silica gives the clusters high dispersibility in water. TiO_2 nanocrystal clusters with an optimal balance of high crystallinity and large surface area can be produced at a calcination temperature of 400 °C, which ensures an enhanced photocatalytic activity as demonstrated by the high charge separation efficiency in electrochemical measurements, and the efficient decomposition of an organic dye under illumination by UV light. The porous structure of the TiO_2 nanocrystal clusters also allows convenient nitrogen doping, which promotes the photocatalytic performance in visible light and natural sunlight. We believe that organizing nanocrystals into mesoporous clusters represents a versatile and useful strategy for designing photocatalysts with enhanced activity and stability.

Acknowledgements

Y. Y. thanks the University of California, Riverside, 3M Company, and the Donors of the Petroleum Research Fund, administered by the American Chemical Society, for support of this research. Financial support of this work was also provided by Basic Energy Sciences–U.S. Department of Energy and the National Science Foundation. Y. Y. is a Cottrell Scholar of the Research Corporation for Science Advancement. We thank Dr. Jimin Shen in Harbin

Institute of Technology (China) for BET measurements. J. B. J. was partially supported by a National Research Foundation of Korea Grant funded by the Korean Government (No. NRF-2009-352-D00056).

References

[1] Fox, M. A.; Dulay, M. T. Heterogeneous photocatalysis. *Chem. Rev.* **1993**, *93*, 341–357.

[2] Kamat, P. V. Photochemistry on nonreactive and reactive (semiconductor) surfaces. *Chem. Rev.* **1993**, *93*, 267–300.

[3] Legrini, O.; Oliveros, E.; Braun, A. M. Photochemical processes for water-treatment. *Chem. Rev.* **1993**, *93*, 671–698.

[4] Kudo, A.; Miseki, Y. Heterogeneous photocatalyst materials for water splitting. *Chem. Soc. Rev.* **2009**, *38*, 253–278.

[5] An, C. H.; Peng, S. N.; Sun, Y. G. Facile synthesis of sunlight-driven AgCl:Ag plasmonic nanophotocatalyst. *Adv. Mater.* **2010**, *22*, 2570–2574.

[6] Fujishima, A.; Honda, K. Electrochemical photolysis of water at a semiconductor electrode. *Nature* **1972**, *238*, 37–38.

[7] Kormann, C.; Bahnemann, D. W.; Hoffmann, M. R. Photolysis of chloroform and other organic-molecules in aqueous TiO_2 suspensions. *Environ. Sci. Tech.* **1991**, *25*, 494–500.

[8] Prairie, M. R.; Evans, L. R.; Stange, B. M.; Martinez, S. L. An investigation of TiO_2 photocatalysis for the treatment of water contaminated with metals and organic-chemicals. *Environ. Sci. Tech.* **1993**, *27*, 1776–1782.

[9] Linsebigler, A. L.; Lu, G. Q.; Yates, J. T. Photocatalysis on TiO_2 surfaces—principles, mechanisms, and selected results. *Chem. Rev.* **1995**, *95*, 735–758.

[10] Hoffmann, M. R.; Martin, S. T.; Choi, W. Y.; Bahnemann, D. W. Environmental applications of semiconductor photocatalysis. *Chem. Rev.* **1995**, *95*, 69–96.

[11] Herrmann, J. M. Heterogeneous photocatalysis: Fundamentals and applications to the removal of various types of aqueous pollutants. *Catal. Today* **1999**, *53*, 115–129.

[12] Tan, S. S.; Zou, L.; Hu, E. Photocatalytic reduction of carbon dioxide into gaseous hydrocarbon using TiO_2 pellets. *Catal. Today* **2006**, *115*, 269–273.

[13] Li, H. X.; Bian, Z. F.; Zhu, J.; Zhang, D. Q.; Li, G. S.; Huo, Y. N.; Li, H.; Lu, Y. F. Mesoporous titania spheres with tunable chamber structure and enhanced photocatalytic activity. *J. Am. Chem. Soc.* **2007**, *129*, 8406–8407.

[14] Chen, X. B. Titanium dioxide nanomaterials and their energy applications. *Chin. J. Catal.* **2009**, *30*, 839–851.

[15] Chen, S. F.; Li, J. P.; Qian, K.; Xu, W. P.; Lu, Y.; Huang, W. X.; Yu, S. H. Large scale photochemical synthesis of M@TiO_2 nanocomposites (M = Ag, Pd, Au, Pt) and their optical properties, CO oxidation performance, and antibacterial effect. *Nano Res.* **2010**, *3*, 244–255.

[16] Ye, M.; Zhang, Q.; Hu, Y.; Ge, J.; Lu, Z.; He, L.; Chen, Z.; Yin, Y. Magnetically recoverable core–shell nanocomposites with enhanced photocatalytic activity. *Chem. Eur. J.* **2010**, *16*, 6243–6250.

[17] Stafford, U.; Gray, K. A.; Kamat, P. V.; Varma, A. An *in situ* diffuse reflectance FTIR investigation of photocatalytic degradation of 4-chlorophenol on a TiO_2 powder surface. *Chem. Phys. Lett.* **1993**, *205*, 55–61.

[18] Riegel, G.; Bolton, J. R. Photocatalytic efficiency variability in TiO_2 particles. *J. Phys. Chem.* **1995**, *99*, 4215–4224.

[19] Hurum, D. C.; Agrios, A. G.; Gray, K. A.; Rajh, T.; Thurnauer, M. C. Explaining the enhanced photocatalytic activity of Degussa P25 mixed-phase TiO_2 using EPR. *J. Phys. Chem. B* **2003**, *107*, 4545–4549.

[20] Zhang, Z. Y.; Zuo, F.; Feng, P. Y. Hard template synthesis of crystalline mesoporous anatase TiO_2 for photocatalytic hydrogen evolution. *J. Mater. Chem.* **2010**, *20*, 2206–2212.

[21] Zhang, L. W.; Fu, H. B.; Zhu, Y. F. Efficient TiO_2 photocatalysts from surface hybridization of TiO_2 particles with graphite-like carbon. *Adv. Funct. Mater.* **2008**, *18*, 2180–2189.

[22] Yun, H. J.; Lee, H.; Joo, J. B.; Kim, W.; Yi, J. Influence of aspect ratio of TiO_2 nanorods on the photocatalytic decomposition of formic acid. *J. Phys. Chem. C* **2009**, *113*, 3050–3055.

[23] Ferrere, S.; Gregg, B. A. Photosensitization of TiO_2 by $[Fe^{II}(2,2'\text{-bipyridine-}4,4'\text{-dicarboxylic acid})_2(CN)_2]$: Band selective electron injection from ultra-short-lived excited states. *J. Am. Chem. Soc.* **1998**, *120*, 843–844.

[24] Adachi, M.; Murata, Y.; Takao, J.; Jiu, J. T.; Sakamoto, M.; Wang, F. M. Highly efficient dye-sensitized solar cells with a titania thin-film electrode composed of a network structure of single-crystal-like TiO_2 nanowires made by the "oriented attachment" mechanism. *J. Am. Chem. Soc.* **2004**, *126*, 14943–14949.

[25] Argazzi, R.; Bignozzi, C. A.; Yang, M.; Hasselmann, G. M.; Meyer, G. J. Solvatochromic dye sensitized nanocrystalline solar cells. *Nano Lett.* **2002**, *2*, 625–628.

[26] Granados-Oliveros, G.; Paez-Mozo, E. A.; Ortega, F. M.; Ferronato, C.; Chovelon, J. M. Degradation of atrazine using metalloporphyrins supported on TiO_2 under visible light irradiation. *Appl. Catal. B* **2009**, *89*, 448–454.

[27] Emeline, A. V.; Kuznetsov, V. N.; Rybchuk, V. K.; Serpone, N. Visible-light-active titania photocatalysts: The case of N-doped TiO_2s—properties and some fundamental issues. *Int. J. Photoenergy* **2008**, Article ID 258394.

[28] Anpo, M.; Takeuchi, M. The design and development of highly reactive titanium oxide photocatalysts operating under visible light irradiation. *J. Catal.* **2003**, *216*, 505–516.

[29] Choi, W. Y.; Termin, A.; Hoffmann, M. R. The role of metal-ion dopants in quantum-sized TiO_2—correlation between photoreactivity and charge-carrier recombination dynamics. *J. Phys. Chem.* **1994**, *98*, 13669–13679.

[30] Li, F. B.; Li, X. Z.; Hou, M. F. Photocatalytic degradation of 2-mercaptobenzothiazole in aqueous La^{3+}–TiO_2 suspension for odor control. *Appl. Catal. B* **2004**, *48*, 185–194.

[31] Sato, S. Photocatalytic activity of NO_x-doped TiO_2 in the visible light region. *Chem. Phys. Lett.* **1986**, *123*, 126–128.

[32] Asahi, R.; Morikawa, T.; Ohwaki, T.; Aoki, K.; Taga, Y. Visible-light photocatalysis in nitrogen-doped titanium oxides. *Science* **2001**, *293*, 269–271.

[33] Sakthivel, S.; Kisch, H. Daylight photocatalysis by carbon-modified titanium dioxide. *Angew. Chem. Int. Ed.* **2003**, *42*, 4908–4911.

[34] Khan, S. U. M.; Al-Shahry, M.; Ingler, W. B. Efficient photochemical water splitting by a chemically modified *n*-TiO_2. *Science* **2002**, *297*, 2243–2245.

[35] Chen, X.; Mao, S. S. Titanium dioxide nanomaterials: Synthesis, properties, modifications, and applications. *Chem. Rev.* **2007**, *107*, 2891–2959.

[36] Chen, D. H.; Huang, F. Z.; Cheng, Y. B.; Caruso, R. A. Mesoporous anatase TiO_2 beads with high surface areas and controllable pore sizes: A superior candidate for high-performance dye-sensitized solar cells. *Adv. Mater.* **2009**, *21*, 2206–2210.

[37] Kim, Y. J.; Lee, M. H.; Kim, H. J.; Lim, G.; Choi, Y. S.; Park, N. G.; Kim, K.; Lee, W. I. Formation of highly efficient dye-sensitized solar cells by hierarchical pore generation with nanoporous TiO_2 spheres. *Adv. Mater.* **2009**, *21*, 3668–3673.

[38] Bai, F.; Wang, D. S.; Huo, Z. Y.; Chen, W.; Liu, L. P.; Liang, X.; Chen, C.; Wang, X.; Peng, Q.; Li, Y. D. A versatile bottom-up assembly approach to colloidal spheres from nanocrystals. *Angew. Chem. Int. Ed.* **2007**, *46*, 6650–6653.

[39] Wang, D. S.; Xie, T.; Peng, Q.; Li, Y. D. Ag, Ag_2S, and Ag_2Se nanocrystals: Synthesis, assembly, and construction of mesoporous structures. *J. Am. Chem. Soc.* **2008**, *130*, 4016–4022.

[40] Lu, Z.; Ye, M.; Li, N.; Zhong, W.; Yin, Y. Self-assembled TiO_2 nanocrystal clusters for selective enrichment of intact phosphorylated proteins. *Angew. Chem. Int. Ed.* **2010**, *49*, 1862–1866.

[41] Lu, Z.; Duan, J.; He, L.; Hu, Y.; Yin, Y. Mesoporous TiO_2 nanocrystal clusters for selective enrichment of phosphopeptides. *Anal. Chem.* **2010**, *82*, 7249–7258.

[42] Lu, Z.; He, L.; Yin, Y. Superparamagnetic nanocrystal clusters for enrichment of low-abundance peptides and proteins. Chem. *Commun.* **2010**, *46*, 6174–6176.

[43] Trentler, T. J.; Denler, T. E.; Bertone, J. F.; Agrawal, A.; Colvin, V. L. Synthesis of TiO_2 nanocrystals by nonhydrolytic solution-based reactions. *J. Am. Chem. Soc.* **1999**, *121*, 1613–1614.

[44] Stober, W.; Fink, A.; Bohn, E. Controlled growth of monodisperse silica spheres in the micron size range. *J. Colloid Interface Sci.* **1968**, *26*, 62–69.

[45] Gribb, A. A.; Banfield, J. F. Particle size effects on transformation kinetics and phase stability in nanocrystalline TiO_2. *Am. Mineral.* **1997**, *82*, 717–728.

[46] Zhang, H. Z.; Banfield, J. F. Thermodynamic analysis of phase stability of nanocrystalline titania. *J. Mater. Chem.* **1998**, *8*, 2073–2076.

[47] Gao, Y. F.; Masuda, Y.; Peng, Z. F.; Yonezawa, T.; Koumoto, K. Room temperature deposition of a TiO_2 thin film from aqueous peroxotitanate solution. *J. Mater. Chem.* **2003**, *13*, 608–613.

[48] Tang, H.; Prasad, K.; Sanjines, R.; Schmid, P. E.; Levy, F. Electrical and optical-properties of TiO_2 anatase thin-films. *J. Appl. Phys.* **1994**, *75*, 2042–2047.